Slag-steel reactions in the refining of Advanced High-Strength Steel

P. Su[1], P.C. Pistorius[2] and B.A. Webler[3]

1. Ph.D. candidate, Carnegie Mellon University, Pittsburgh PA 15213, U.S.A.
   Email: panwens@andrew.cmu.edu
2. POSCO Professor, Carnegie Mellon University, Pittsburgh PA 15213, U.S.A.
   Email: pistorius@cmu.edu
3. Professor, Carnegie Mellon University, Pittsburgh PA 15213, U.S.A.
   Email: webler@cmu.edu

ABSTRACT

Advanced high-strength steels typically have much higher aluminum concentrations (by an order of magnitude or more) than conventional low-carbon aluminum-killed steels. The resulting lower oxygen activity at the steel-slag interface changes the kinetics and thermodynamics of steel-slag reactions. Previous work showed that the rapid transformation of alumina inclusions to spinel inclusions, and spinel to periclase, occurs - because of the relatively high concentration of dissolved magnesium. In this paper, experimental results on nitrogen removal by ladle slag are compared with predictions based on the available thermodynamic databases. As in previous work, the kinetics was modeled by assuming mass transfer control, with steel or slag mass transfer limiting. The results show that significant removal of nitrogen by steel-slag reaction is possible.
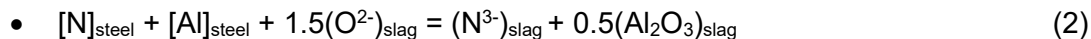
INTRODUCTION

The third-generation advanced high-strength steels (3rd GEN AHSS), with ≥ 1 GPa tensile strength and ~30% elongation ("Advanced High-Strength Steel (AHSS) Definitions," n.d.), contain intermediate levels of alloying elements (0.05 to 0.5%C, 0-4% Al, 0-12 % Mn, and 0-4% Si) (Tang and Pistorius, 2021). Nitrogen control is important for steel quality: Al, Si, and Mn are strong nitride formers (Paek et al., 2016). The resulting high solubility of nitrogen in these steels precludes nitrogen removal by vacuum degassing (Tang and Pistorius, 2022). A method was proposed to remove nitrogen by intentionally forming AlN precipitates that can be removed in the slag (Tada and Matsumura, 2011), but the AlN precipitates may redissolve before leaving the liquid steel. Instead, in the work presented here, the focus is on slag-based nitrogen removal from liquid 3rd GEN AHSS, using conventional calcium aluminate ladle slag. To study nitrogen removal, thermodynamic and kinetics calculations with FactSage 8.1 (Bale et al., 2016) and laboratory experiments with liquid steel and slag were employed.

For the conditions in this work (steel, not carbon saturated, temperature around 1600 °C, CaO-rich slag), nitrogen can dissolve in the slag by the following reactions: (Jung, 2006)

- $[N]_{steel} + 1.5(O^{2-})_{slag} = 0.75\ O_2 + (N^{3-})_{slag}$ (1a)

- $[Al]_{steel} + 0.75\ O_2 = 0.5(Al_2O_3)_{slag}$ (1b)

Combination of reactions (1a) and (1b) gives the following net reaction:

- $[N]_{steel} + [Al]_{steel} + 1.5(O^{2-})_{slag} = (N^{3-})_{slag} + 0.5(Al_2O_3)_{slag}$ (2)

Reaction (2) illustrates why nitrogen removal by slag from AHSS steels might be feasible: the high aluminum concentration in these steels (one to two orders of magnitude higher than in conventional low-carbon aluminum-killed steel) would drive the nitrogen removal reaction to the right.

The high aluminum concentration in such steels leads to rapid transformation of alumina (initial deoxidation production), to spinel (approximately $MgAl_2O_4$), and periclase (MgO). The rapid transformation results from the relatively high concentration of dissolved magnesium (several tens of parts per million) at the steel-slag interface (Tang and Pistorius, 2021).

CALCULATIONS AND EXPERIMENTAL PROCEDURE

Kinetics Calculations

The expected rate of steel-slag reactions – for the conditions of the laboratory trials – was calculated based on the assumption that mass transfer in the steel or slag (to the steel-slag interface) was rate-controlling, with local equilibrium at the steel-slag interface. The calculations were performed with FactSage macros, based on the effective equilibrium reaction zone (EERZ) approach (Van Ende et al., 2011): within a chosen time interval, portions of slag and steel are transported to the slag-steel interface to equilibrate; the amount of the phase reacting is equal to the product of the time interval, the effective mass transfer coefficient, the projected slag-steel area, and the density of the phase (Pistorius and Vermaak, 1999). After equilibration, the reaction products are mixed back into the slag and steel, and each phase is homogenized. Gaseous reactions were not considered, given the low rate of gas-based removal of nitrogen from AHSS (Tang and Pistorius, 2022). The databases and parameters employed for the FactSage simulations are listed in Table 1. The initial slag and steel

compositions for the simulations and for the laboratory slag-steel reactions are given in Tables 2 and 3. The slag compositions were chosen to be close to double saturation with both periclase and lime (based on FactSage calculations), with different initial SiO_2 concentrations. The FTOxCN slag database was found to agree with previous experimental results for slag-based nitrogen removal (Jung, 2006) (albeit not for higher-Al steels as considered in this work).

For reactions involving substantial transfer of oxygen between slag and steel (as in this work, due to reduction of SiO_2 from the slag, by reaction with Al in the metal), emulsification can be expected at the slag-steel interface (Riboud and Lucas, 1981) (Assis et al., 2015) (Song et al., 2021). To approximate the observed time constants of the steel-slag reactions, it was necessary to increase the interfacial area in the simulations (to be larger than the cross-sectional area of the crucible); the extent of this increase is given by the column "A/A_0" in Table 3.

To match the final Al and Si concentrations in the steel, it was needed to add additional oxygen to the initial steel composition, for the kinetic simulations. This reflects entry of oxygen into the furnace chamber when the slag is added. The total oxygen load in the steel at the start of steel-slag reaction was taken to be 2000 ppm for the results shown here.

TABLE 1 – Solution Models and Simulation Parameters for Modeling Slag-Steel Reactions

Phase	Solution model	
Liquid steel	FTmisc FeLQ	
Slag	FTOxCN-slag	
Solid oxides	FToxid-A-monoxide; FToxid-B-spinel; FToxid-corundum; FToxid-a-$(Ca,Sr)_2SiO_4$	
Simulation parameters	Slag density, ρ_{slag}	2500 kg/m^3
	Steel density, ρ_{steel}	7000 kg/m^3
	Slag-to-steel mass ratio	1:5 to 1:12
	Steel mass transfer coefficient, m_{steel}	3.1×10^{-5} m/s (Piva and Pistorius, 2021)
	Slag mass transfer coefficient, m_{slag}	$0.1 m_{steel}$

TABLE 2 – Initial Steel Compositions for Simulations and Steel-Slag Reactions (Mass Percentages)

Version	Fe	Al	C	Mn	N	O	S	Si
High Al	Balance	0.83	0.2	2.1	0.002-0.02	0.01	~0.001	0.45
Low Al	Balance	0.087	0.2	2.1	0.002-0.02	0.01/0.15	~0.001	0.45

TABLE 3 – Initial slag compositions and temperatures for experiments and simulations, with the experimental steel-to-slag mass ratio and the estimated increase in slag area by emulsification (A/A_0)

Experiment	T (^{O}C)	%Al_2O_3	%CaO	%MgO	%SiO_2	W_{steel}/W_{slag}	A/A_0
E1	1550	35	54	6	5	12.8	5
E2	1600	42.3	51.2	6.5	0	6.3	2
E3	1600	36.9	53.5	5.6	4	4.6	2
E4	1600	35	54	6	5	5.0	1.5
E5	1600	42.3	51.2	6.5	0	5.3	2
E6	1600	42.3	51.2	6.5	0	5.0	5

Note: Experiments E1 to E5 used the higher-Al steel (0.83% Al before reaction), while E6 used the lower-Al steel (0.087% Al before reaction).

Slag-Steel Reactions

Experiments were performed in an induction furnace, as described previously (Mu et al., 2018; Piva et al., 2017; Roy et al., 2013; Song et al., 2021). Experiments were performed in slip-cast MgO crucibles (OD = 64 mm, ID = 56 mm, height = 138 mm), using approximately 600 g of metal and 120 g of slag, in a high-purity argon atmosphere (flow rate ~0.6 dm^3/min at room temperature and ambient pressure). Raw materials for the metal were placed into the crucible before the experiment. Electrolytic iron (with ~400 ppm O, based on previous work (Piva et al., 2017)), Al shot, graphite

powder, electrolytic Mn pieces, pure Si pieces, and crushed pieces of nitrided electrolytic manganese were used to make up the metal composition. Although the nominal nitrogen concentration in the nitrided manganese was approximately 6%, the actual nitrogen at melt-in varied (likely because of inhomogeneity of the manganese briquettes), as the results show.

Slag for the experiments was prepared from pure oxides that were mixed, pressed into pellets, and then premelted in a graphite crucible under argon (heating to and holding at approximately 1600 °C for 10 minutes). After cooling to room temperature, the graphite crucible was broken to remove the premelted slag. The slag was broken up, and ground using a tungsten carbide puck mill. Following grinding, the slag was decarburized in air at 1000 °C for 24 h. The decarburized slag powder was then pelletized and sintered at 1000 °C for 12 h in an alumina crucible (62×56×60 mm) before the slag-steel experiments.

The slag-steel reactions were conducted in an induction furnace (maximum power = 10 kW). The MgO crucible containing the steel was placed in a graphite susceptor (OD = 71.5 mm, ID = 65.5 mm, height = 160 mm, bottom thickness = 15 mm) on an insulating alumina pedestal. Alumina felt was used as thermal insulation around the outside of the susceptor. A disc cut from porous alumina brick was used as a radiation shield on top of the crucible (with holes through which the sheath of the upper thermocouple and the feeding tube passed). The atmosphere was controlled by enclosing the susceptor in a fused-quartz tube (80 mm ID, 85 mm OD, 430 mm long), with a water-cooled stainless-steel end cap sealing onto Viton gaskets at each end of the fused-quartz tube. Temperature was monitored with both upper and lower B-type thermocouples, sheathed with 6.35 mm OD alumina tubes. The sheathed tip of the bottom thermocouple (B-type) ended in a shallow hole (7.5 mm diameter, 9 mm deep) in the bottom center of the graphite susceptor. The offset between the reading of the bottom thermocouple and the interior of the MgO crucible was measured with an empty crucible, and found to be approximately 150 °C. The tip of the upper thermocouple was placed approximately 5 mm above the estimated top of the slag layer. An alumina feeding tube passed through the upper end cap and was sealed with a silicone rubber stopper when slag was not being fed into the crucible.

After charging the crucible and sealing the working tube with the end caps, the crucible with the steel mixture was heated to the experimental temperature (1600 °C for all but the first case; see Table 3) at a rate of approximately 30 K/min, by manually adjusting the power of the induction supply. The steel was held for 10 minutes for melting and homogenization, before taking the first steel sample.

Steel rod samples were taken by inserting the tip of a fused-quartz tube (4 mm ID, 6.35 mm OD, length 600 mm) through the feeding tube into the crucible, and using a manual pipette pump to draw liquid steel into the fused-quartz tube.

After taking the first steel sample, slag pieces (diameter ≤ 3 mm) were added to the crucible through the unplugged feeding tube. The addition took several minutes, during which time the Ar flow was turned off to avoid slag powder blowing out of the feeding tube. During slag addition, oxygen would have entered the working tube, affecting the aluminum balance (as mentioned earlier). After slag addition, the feeding tube was sealed with the silicone stopper and Ar flow restarted at 0.6 dm^3/min. The system was subsequently held for ~10 minutes for complete melting of the slag, before taking the first sample after slag addition. Several samples were taken subsequently while maintaining a constant temperature, for total times up to 3 hours.

The nitrogen concentrations in the steel rod samples were analyzed by IGA (instrumental gas analysis) at an external laboratory. The steel remaining in the crucible was analyzed at another laboratory, using spark optical emission spectroscopy (OES) for all elements other than nitrogen, and IGA for nitrogen. Slag was manually separated from the crucible, crushed and analyzed by X-ray fluorescence (for all except experiment E6). Given uncertainties around the analysis of nitrogen in slag, the analyzed nitrogen concentration in the steel was used to calculate the nitrogen distribution coefficient between the steel and slag, as follows:

The nitrogen distribution coefficient is given by:

$$L_N = (\%N)_{slag}/[\%N]_{steel}, \tag{3}$$

where $(\%N)_{slag}$ is the mass percentage of nitrogen in the slag, and $[\%N]_{steel}$ is the mass percentage of nitrogen in the steel. From a simple mass balance, based on the assumptions that the steel and

4

slag are homogeneous, and that the slag contained no nitrogen before reaction, the nitrogen distribution coefficient after the steel-slag reaction can be calculated as follows from the measured steel compositions:

$$L_N = ([\%N]_i/[\%N]_f - 1)\,(W_{steel}/W_{slag}), \qquad (4)$$

where $[\%N]_i$ is the nitrogen concentration in the steel before reaction, $[\%N]_f$ the nitrogen concentration after reaction, and W_{steel} and W_{slag} are the total masses of steel and slag.

Microscopy

Selected steel and slag samples were examined by scanning electron microscopy after the experiments. To test for possible AlN formation, a steel rod sample (N content = 190 ppm as given by IGA analysis) was mounted in conductive bakelite and polished to a 1 μm finish with diamond. Possible slag-crucible reactions were examined by mounting a piece of crucible (with attached slag) in cold-mounting epoxy resin, followed by grinding and polishing (with diamond) while avoiding any contact with water. Samples were examined by back-scattered electron imaging, using an accelerating voltage of 10 kV. The slag sample was carbon-coated before microscopy.

RESULTS AND DISCUSSION

Extent of steel-slag reactions

The time variation of %N in steel, for both FactSage simulations and experiments, are given in Fig. 1; the measured steel and slag compositions after reaction are given in Tables 4 and 5. The measured MgO concentration in the samples of runs E2-E4 was much higher than expected for MgO-saturated slags; a likely reason is incomplete separation of slag from the MgO crucible before the slag was crushed for XRF analysis.

Note that a large decrease in aluminum concentration occurred (from around 0.9% to 0.4%, for experiments E1 to E5), with a slight increase in silicon concentration in the steel (from 0.45% to around 0.6% on average), and greatly reduced silica concentration in the slag. However, the decrease in [%Al] is larger than can be accounted for just by the reduction of SiO_2: From stoichiometry, the reaction of 4 moles of Al with 3 moles of SiO_2 would yield 3 moles of Si (and 2 moles of Al_2O_3), with result that the ratio of the change in [%Al] to the change in [%Si] would be -1.3. The larger observed ratio of the aluminum to silicon changes (around -3) indicates that additional oxygen entered the experiment, causing additional loss of aluminum from the steel; this is also shown by the decrease of both [%Al and [%Si] in the low-Al experiment (E6). As mentioned earlier, oxygen likely entered during slag addition. The resulting loss of aluminum would have decreased the extent of nitrogen removal (as shown by Reaction 2). (As Reaction 2 indicates, some Al would also have been consumed by the nitrogen removal reaction, but this amount is small: given the 1:1 stoichiometry of Al and N in the reaction, removal of up to 200 ppm N would have resulted in consumption of less than 400 ppm of Al.)

Despite the loss of aluminum, substantial nitrogen removal did occur, as illustrated by Figure 1, and by the summary of nitrogen distribution coefficients in Table 6. The extent of nitrogen removal was insignificant only in the case of the low-Al control experiment (E6; distribution coefficient approximately 2). In the cases with higher final [%Al], the L_N values were much larger.

The strong effect of [%Al] on nitrogen removal is emphasized by Figure 2, which shows the experimental L_N values for the different final [%Al]. The relationship is scattered, because not only [%Al] varied between experiments, but also slag composition – which would have changed the activities of Al_2O_3 and O^{2-} and the N^{3-} activity coefficients in the slag. Despite the scatter, fitting a power-law expression to the data shows that L_N is approximately proportional to [%Al] (the fitted exponent is 1.17, similar to the expected value of 1). The conclusion is that nitrogen can be removed from high-Al AHSS by reaction with ladle slag.

The extent of nitrogen removal in the experiments was large also because of the high mass ratio of slag to steel. This high mass ratio was essential to ensure that the steel was fully covered by slag. However, significant nitrogen removal would also be possible under industrial conditions, with much lower slag-to-steel mass ratios. Taking a typical ladle slag to steel mass ratio of $W_{slag}/W_{steel} = 0.015$,

and L_N = 60 (feasible for [%Al]=1%, as indicated by the experiments), the fraction of nitrogen removed from the steel (if the slag contained zero nitrogen before reaction) would be $1 - 1/(1+L_N W_{slag}/W_{steel})$ = 0.47. That is, approximately half of the nitrogen would be removed from the steel.

Figure 1 indicates that the observed time constants for nitrogen removal could be matched approximately by increasing the modeled steel-slag interfacial area (by the factors listed in Table 3). This increased area is expected for a system such as this, where high-Al steel reduces SiO_2 from the slag (Riboud and Lucas, 1981).

However, Figure 1 indicates that the observed extent of nitrogen removal was smaller than that predicted with FactSage. Part of this difference is due to the larger-than-predicted loss of aluminum due to the presumed ingress of oxygen. However, even when compensating for the loss of Al, the observed nitrogen distribution coefficients are generally smaller than those predicted by FactSage, as illustrated by Table 6. The conclusion is that, while the FactSage databases used here give useful indications of the reaction trends, the actual nitrogen removal – while substantial – would be less than predicted.

Table 4. The final steel composition after slag-steel experiments (nitrogen measured by IGA; other elements by spark OES; mass concentrations)

Experiment	Al pct	C pct	Mn pct	Mg (ppm)	Si pct	N (ppm)
E1	0.33	0.19	2.0	43	0.63	4.1
E2	0.41	0.15	1.9	49	0.53	3.4
E3	0.11	0.14	2.0	15	0.78	10
E4	0.36	0.20	2.4	71	0.58	47
E5	0.48	0.19	2.6	44	0.54	31
E6	0.06	0.20	2.4	12	0.37	101

Table 5. Initial slag compositions (double-saturated with CaO and MgO, based on FactSage) and the actual final slag compositions as analyzed by XRF.

Slag	Al_2O_3%		CaO%		MgO%		SiO_2%	
	Initial	Final	Initial	Final	Initial	Final	Initial	Final
E1	35.6	42.53	53.95	48.66	5.45	7.72	5	1.09
E2	41.81	42.9	51.04	45.72	7.15	10.41	0	0.97
E3	36.45	33.6	53.26	40.61	6.29	24.97	4	0.81
E4	35.15	29.04	53.71	39.29	6.14	30.4	5	1.27
E5	41.81	43.98	51.04	49.42	7.15	6.61	0	0

Table 6. Nitrogen distribution coefficients between slag and steel, as predicted from FactSage, and observed in experiments.

Experiment	[N]$_{initial,}$ ppm	[N]$_{final}$, ppm		W_{steel}/W_{slag}	L_N	
		FactSage	Expt.		FactSage	Expt.
E1	25	3.5	4.6	12.8	79	56.8
E2	50	3.8	3.4	6.3	77	86.3
E3	46	5.0	10.3	4.6	38	15.9
E4	93	12.9	32.0	5.0	31	9.5
E5	190	12.9	30.5	5.3	73	27.7
E6	150	53/80 (for initial [O] 100/1500 ppm)	101	5.0	9.2/4.3 (for initial [O] 100/1500 ppm)	2.4

Slag microstructure

The solidified slag (after reaction with the Al-bearing steel at 1600 °C) (Figure 3) contained the expected phases. As noted in Table 1, matching the observed nitrogen removal rate required increasing the effective steel-slag contact area by a factor of 2 (for the slag example in Figure 3).

However, no emulsification was observed in the steel and slag after the experiments, likely because of the long duration of the experiments: Once the steel-slag reactions cease, no driving force for emulsification remains.

Aluminum nitride in solidified steel

Given the high Al and N concentrations in the experimental steels (before nitrogen removal by the slag), the solid AlN may form in the steel (Paek et al., 2013). Scanning electron microscopy (10 kV accelerating voltage) of the first sample taken from Run E5 (containing 190 ppm) did show the presence of small AlN precipitates; examples are given in Figure 4. In some cases, the AlN appeared to have precipitated on an MgO-containing oxide core, as indicated by the energy dispersive X-ray (EDX) spectra in the figure. The predicted phase equilibria, calculated with Thermo-Calc 2024a (TCFE13 database) (Andersson et al., 2002) support the formation AlN during solidification (Figure 5). While some AlN forms during solidification, it is not stable in the liquid steel during ladle treatment (for the compositions considered here) and does not contribute to nitrogen removal during steel refining.
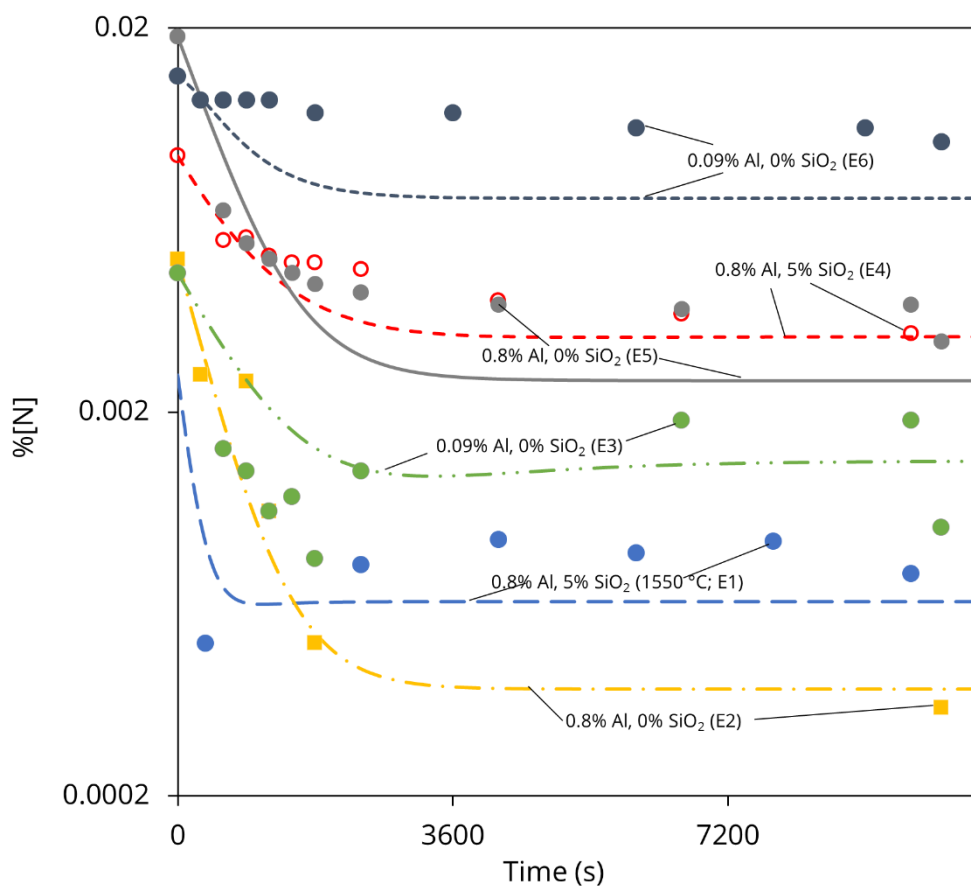

FIG 1 – Change in [%N] over time, for slag-steel experiments. Markers show the experimental results, and the lines the results of FactSage simulations.
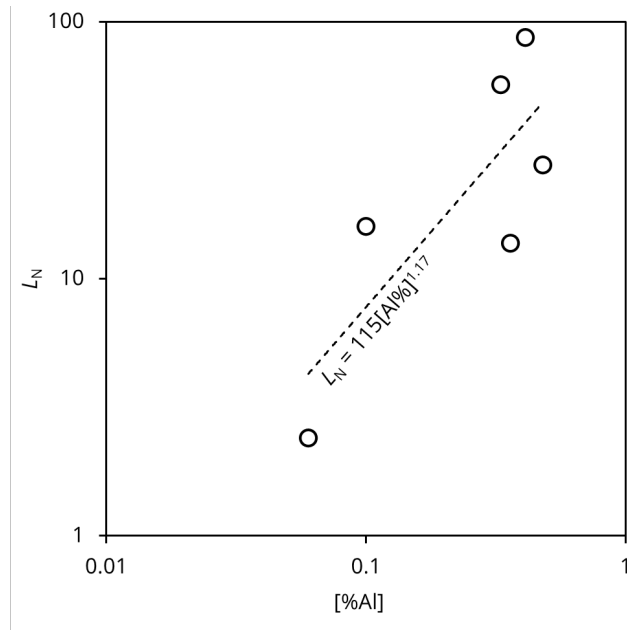
FIG 2 – Observed relationship between the nitrogen distribution coefficient and the final Al concentration in the steel, for all the experiments.
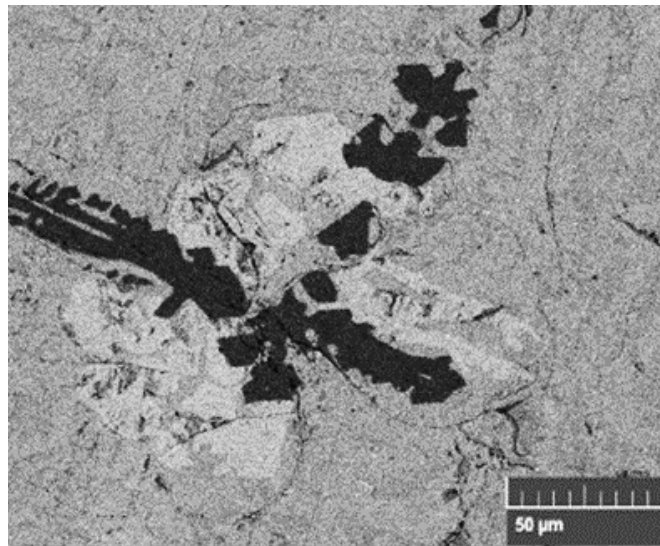

FIG 3 – SEM-BSE image of the 0% SiO_2 slag after reaction at 1600 °C with higher-Al steel (E5). The major phases are $Ca_3Al_2O_6$ (brightest phase), $Ca_3MgAl_4O_{10}$ (mid-grey region), and MgO (darkest dendrites).
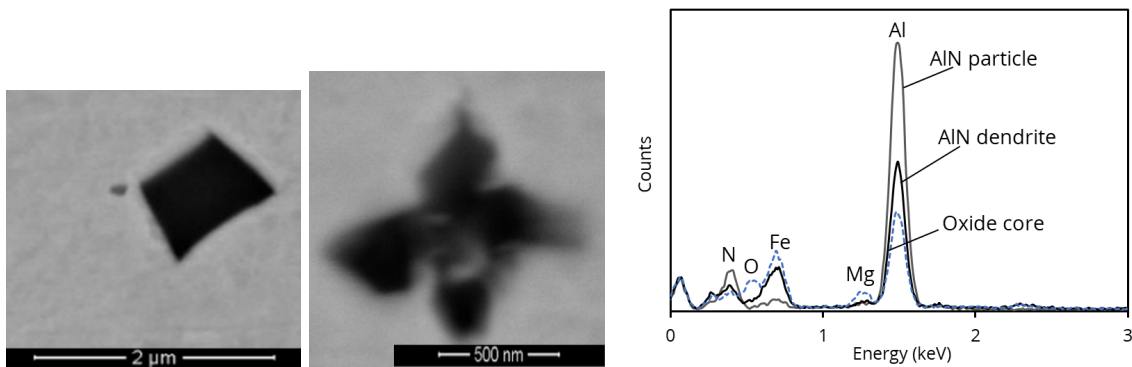

FIG 4 – Backscattered electron micrographs of AlN precipitates in the first steel sample from run E5, with EDX spectra at right.
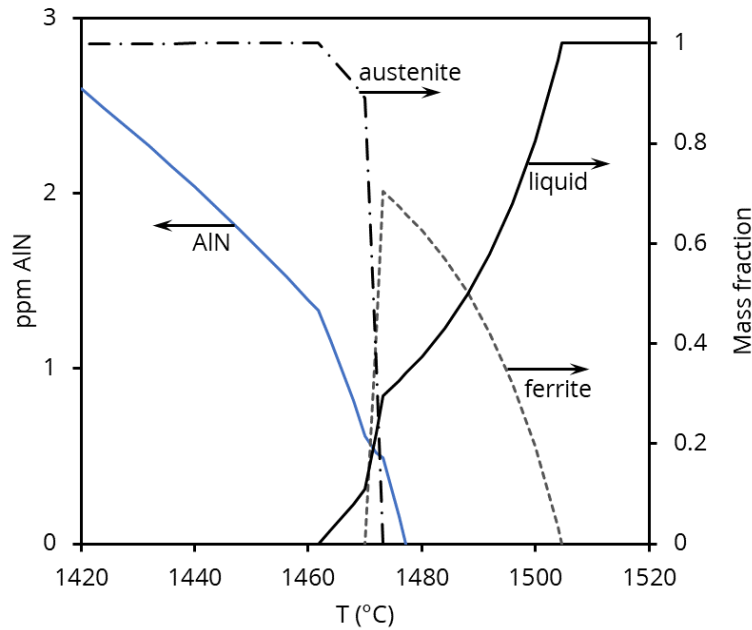
FIG 5 – Calculated equilibrium phases in the steel of run E5, with 190 ppm nitrogen.

Comparison of IGA and OES analysis of nitrogen in steel

Optical emission spectroscopy (OES) provides rapid analyses, but is less accurate for low concentrations of nitrogen. However, comparison of the reported compositions of the final steel samples (Table 7) shows close agreement between the IGA and OES results, for samples containing more than approximately 30 ppm nitrogen. This indicates that suitably calibrated OES can be used to rapidly assess nitrogen removal (or pick-up) during industrial ladle processing of liquid steel.

Table 7. Comparison of nitrogen analyses of the final steel samples, obtained by IGA and Spark-OES

Experiment	N ppm, IGA	N ppm, Spark OES
E1	4.6	<5
E2	3.4	<5
E3	10.3	13.6
E4	32	32
E5	32	37
E6	110	101

CONCLUSIONS

Considerable nitrogen removal with calcium aluminate slag is possible during the ladle processing of AHSS containing >0.1% dissolved aluminum. The available FactSage database provides a useful indication of the expected reactions, though it slightly overpredicts the extent of nitrogen removal.

ACKNOWLEDGEMENTS

REFERENCES

Advanced High-Strength Steel (AHSS) Definitions [WWW Document], n.d. . WorldAutoSteel. URL
        https://www.worldautosteel.org/steel-basics/automotive-advanced-high-strength-steel-ahss-definitions/
        (accessed 4.13.24).
Andersson, J.-O., Helander, T., Höglund, L., Shi, P., Sundman, B., 2002. Thermo-Calc & DICTRA, computational tools
        for materials science. Calphad 26, 273–312. https://doi.org/10.1016/S0364-5916(02)00037-8

Assis, A.N., Warnett, J., Spooner, S., Fruehan, R.J., Williams, M.A., Sridhar, S., 2015. Spontaneous Emulsification of a Metal Drop Immersed in Slag Due to Dephosphorization: Surface Area Quantification. Metall Mater Trans B 46, 568–576. https://doi.org/10.1007/s11663-014-0248-z

Bale, C.W., Bélisle, E., Chartrand, P., Decterov, S.A., Eriksson, G., Gheribi, A.E., Hack, K., Jung, I.-H., Kang, Y.-B., Melançon, J., Pelton, A.D., Petersen, S., Robelin, C., Sangster, J., Spencer, P., Van Ende, M.-A., 2016. FactSage thermochemical software and databases, 2010–2016. Calphad 54, 35–53. https://doi.org/10.1016/j.calphad.2016.05.002

Jung, I.-H., 2006. Thermodynamic Modeling of Gas Solubility In Molten Slags (I) - Carbon and Nitrogen. ISIJ International 46, 1577–1586. https://doi.org/10.2355/isijinternational.46.1577

Mu, H., Zhang, T., Fruehan, R.J., Webler, B.A., 2018. Reduction of CaO and MgO Slag Components by Al in Liquid Fe. Metall Mater Trans B 49, 1665–1674. https://doi.org/10.1007/s11663-018-1294-8

Paek, M.-K., Chatterjee, S., Pak, J.-J., Jung, I.-H., 2016. Thermodynamics of Nitrogen in Fe-Mn-Al-Si-C Alloy Melts. Metall Mater Trans B 47, 1243–1262. https://doi.org/10.1007/s11663-016-0588-y

Paek, M.-K., Jang, J.-M., Jiang, M., Pak, J.-J., 2013. Thermodynamics of AlN Formation in High Manganese-Aluminum Alloyed Liquid Steels. ISIJ Int. 53, 973–978. https://doi.org/10.2355/isijinternational.53.973

Pistorius, P., Vermaak, M., 1999. Modelling pyro metallurgical kinetics: ladle desulphurization. South African Journal of Science 95, 377–380.

Piva, S.P.T., Kumar, D., Pistorius, P.C., 2017. Modeling Manganese Silicate Inclusion Composition Changes during Ladle Treatment Using FactSage Macros. Metall and Materi Trans B 48, 37–45. https://doi.org/10.1007/s11663-016-0764-0

Piva, S.P.T., Pistorius, P.C., 2021. Ferrosilicon-Based Calcium Treatment of Aluminum-Killed and Silicomanganese-Killed Steels. Metall Mater Trans B 52, 6–16. https://doi.org/10.1007/s11663-020-02017-1

Riboud, P.V., Lucas, L.D., 1981. Influence of Mass Transfer Upon Surface Phenomena in Iron and Steelmaking. Canadian Metallurgical Quarterly 20, 199–208. https://doi.org/10.1179/cmq.1981.20.2.199

Roy, D., Pistorius, P.C., Fruehan, R.J., 2013. Effect of Silicon on the Desulfurization of Al-Killed Steels: Part II. Experimental Results and Plant Trials. Metall Mater Trans B 44, 1095–1104. https://doi.org/10.1007/s11663-013-9888-7

Song, S., Tang, D., Kumar, D., Pistorius, P.C., 2021. Recycling of Chromium-Containing Waste Oxide as Alloying Addition in Ladle Metallurgy. Metall Mater Trans B 52, 2612–2618. https://doi.org/10.1007/s11663-021-02212-8

Tada, C., Matsumura, C., 2011. Removal method of nitrogen in molten steel. US 7,901,482 B2.

Tang, D., Pistorius, P.C., 2021. Non-metallic Inclusion Evolution in a Liquid Third-Generation Advanced High-Strength Steel in Contact with Double-Saturated Slag. Metall Mater Trans B 52, 580–585. https://doi.org/10.1007/s11663-021-02084-y

Tang, D., Pistorius, P.C., 2022. Kinetics of Nitrogen Removal from Liquid Third Generation Advanced High-Strength Steel by Tank Degassing. Metall Mater Trans B. https://doi.org/10.1007/s11663-021-02417-x

Van Ende, M.-A., Kim, Y.-M., Cho, M.-K., Choi, J., Jung, I.-H., 2011. A Kinetic Model for the Ruhrstahl Heraeus (RH) Degassing Process. Metall Mater Trans B 42, 477–489. https://doi.org/10.1007/s11663-011-9495-4